# AN ASSESSMENT OF DEVELOPED THERMOCHROMIC SOLAR FILMS FOR ENERGY CONSERVATION

An Undergraduate Research Scholars Thesis

by

AYSHA MELHIM

Submitted to the LAUNCH: Undergraduate Research office at
Texas A&M University
in partial fulfillment of requirements for the designation as an

UNDERGRADUATE RESEARCH SCHOLAR

Approved by
Faculty Research Advisors: Dr. Mohammed Al-Hashimi
Dr. Sarbajit Banerjee

May 2022

Major: Chemical Engineering

# RESEARCH COMPLIANCE CERTIFICATION

Research activities involving the use of human subjects, vertebrate animals, and/or biohazards must be reviewed and approved by the appropriate Texas A&M University regulatory research committee (i.e., IRB, IACUC, IBC) before the activity can commence. This requirement applies to activities conducted at Texas A&M and to activities conducted at non-Texas A&M facilities or institutions. In both cases, students are responsible for working with the relevant Texas A&M research compliance program to ensure and document that all Texas A&M compliance obligations are met before the study begins.

I, Aysha Melhim, certify that all research compliance requirements related to this Undergraduate Research Scholars thesis have been addressed with my Research Faculty Advisors prior to the collection of any data used in this final thesis submission.

This project did not require approval from the Texas A&M University Research Compliance & Biosafety office.

# TABLE OF CONTENTS

# ABSTRACT

An Assessment of Developed Thermochromic Solar Films for Energy Conservation

Aysha Melhim
Department of Chemical Engineering
Texas A&M University

Research Faculty Advisor: Dr. Mohammed Al-Hashimi
Department of Science
Texas A&M University

Research Faculty Advisor: Dr. Sarbajit Banerjee
Department of Chemistry
Texas A&M University

Energy consumption has become directly associated with buildings. According to the United Nations, it is estimated that buildings contribute by 30-40% of the worldwide energy consumption. The consumption of energy has increased due to urbanization in the past 20 years. Heating, cooling, in addition to external and internal heat gains are, primarily, the source of energy consumption in buildings. Solar heat gains and losses occur through several components of the buildings. For instance, the use of glass windows for indoor lighting. This research aims to assess developed thermochromic nanocomposite films that have been produced through the annealing of Vanadium Dioxide ($VO_2$) nanocrystals within Silicon Dioxide ($SiO_2$) shells. The nanocomposite solar films can spectrally select and dynamically tune control over the visible and infrared regions of the solar spectrum, allowing for control of the desired lighting and solar heat

gain. The control of the light and heat will, consequently, lower energy consumption for heating and cooling in buildings.

# ACKNOWLEDGEMENTS


## Contributors

I would like to thank my faculty advisors, Dr. Mohammed Al-Hashimi and Dr. Sarbajit Banerjee, for their guidance and support throughout the course of this research.

Thanks also go to my friends and colleagues and the department faculty and staff for making my time at Texas A&M University a great experience.

Finally, thanks to Dr. Alexandre Amato for their encouragement and help throughout the project.

All other work conducted for the thesis was completed by the student independently.

## Funding Sources

No funding was received for this project.

# 1. INTRODUCTION

Energy is largely consumed through buildings, therefore increasing their operating costs. The Department of Energy in the United States estimates that buildings consume 41% of the nationwide energy consumption.[1,2] In addition, the American Council for an Energy-Efficient Economy estimates that home air-conditioning alone costs $15B annually and generates 140M tons of Carbon Dioxide ($CO_2$).[3] The world's need for a remedy that can mitigate this excessive energy consumption problem to normal levels is clear. The incorporation of smart elements that can respond and adapt to external stimuli (humidity, external temperature, etc.) within structural elements has been proposed for the reduction of the energy footprint.[3] These elements are expected to modulate the solar heat gains to desired levels. This indicates the importance and interest in energy use regulations for sustainability. Furthermore, a research report conducted via IDTechEx indicated that smart glass will be a $6.5B market by 2028; showing its great economic viability.[4]

In North Africa, commercial and residential buildings have been installed with thermochromic windows. The companies, Suntuitive [5] and Ravenwindow [6], are the major suppliers of these films. However, they were accompanied with technological limitations, such as the limited spectrum coverage, and high thermochromic transition temperatures above 65°C limiting its usage to hot weather only.

We have identified several challenges with the existing thermochromic material and are developing hybrid nanocomposite material with specific criteria. The criteria are, but not limited to, reducing utility costs, carbon footprint of buildings, peak load in summers/hot climates, and the better use of daylight inside buildings.

This research is complimentary and a part of the on-going project by Dr. Al-Hashimi and his team (including myself).

## 1.1 Polymeric Smart Coating Description

The coating is designed to be a color-tunable thermochromic matrix that is programmed to be sensitive to changes in the ambient temperature in the visible light and infrared regions in the solar spectrum. The coating utilizes the reversible electronic metal to insulator and insulator to metal phase transition in $VO_2$. The phase change in $VO_2$ is associated with a structural transition depending on the critical temperature $T_c$. Above the $T_c$ (68ºC for $VO_2$)[7], $VO_2$ is in the rutile metallic phase, which reflects the infrared radiation and below $T_c$, $VO_2$ becomes in the monoclinic phase, which transmits the infrared radiation as illustrated in **Figure 1.1**.

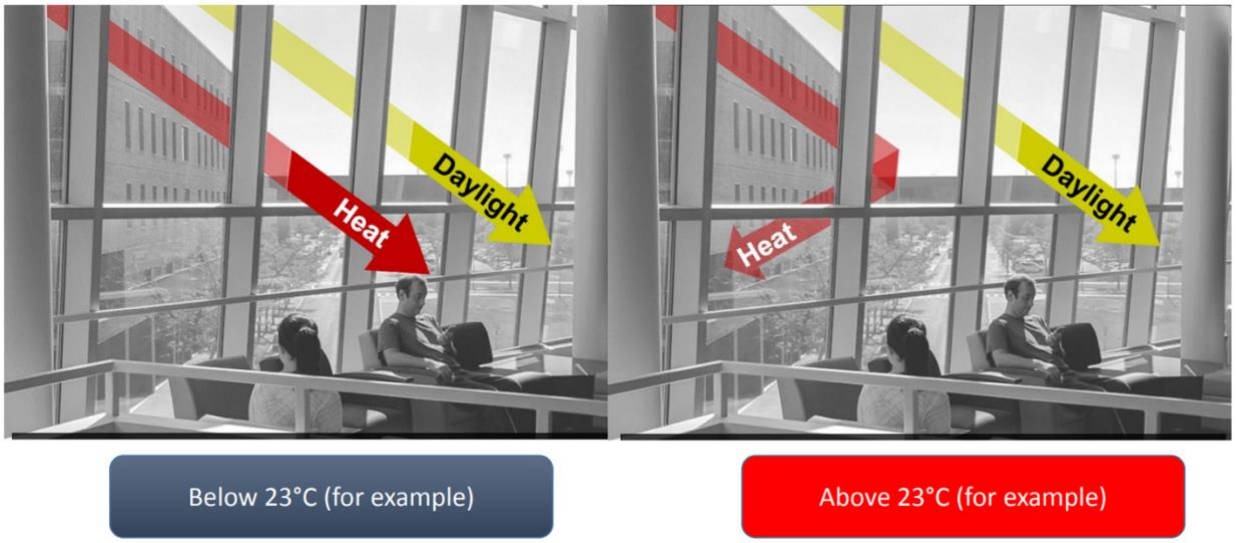


***Figure 1.1**: Illustration of how light is transmitted or reflected based on the transition temperature of the film.*

When the phase transition from insulator to metal occurs in $VO_2$, the near-infrared transmittance is repressed due to the increase in the carrier density associated with metallization causing a drastic increase in the reflected incident solar radiation. Heat gain in buildings is largely

contributed to by the near-infrared radiation and it does not affect the lighting in the interiors of the building as it is not discernible to the naked eyes. This allows for the ability to selectively modulate and control the solar heat gain, which is a function of ambient temperature; therefore, allowing for possible energy conservations, specifically, in the reduction of air-conditioning costs and allowing the utilization of the natural daylight for interior lighting instead of the dependence on energy.

## 1.2 Polymer Description Obtained from Preliminary Data

Over the last years, some improvements on the smart film were developed to enhance the window's energy efficiency. First, the insulator-metal transition of the $VO_2$ can be regenerated with no degradation of the material.[8,9,10] In addition, $VO_2$ nanostructures were developed using a solution-phase hydrothermal route. The nanostructures exhibited insulator-metal transitions that exceeded four times the magnitude at the 10 grams scale; also exceeding the $VO_2$ films' quality that are developed by the physical deposition methods as shown in **Figure 1.2.A-E**. [9,10]

Furthermore, the tunability of the transition temperature was observed and demonstrated in the range of -20 to 70ºC after the addition of dopants, such as boron, molybdenum, and tungsten (refer to **Figure 1.2**).[9,11] The deposition of $SiO_2$ shell and surface functionalizing were demonstrated to protect the $VO_2$ from oxidizing to $V_2O_5$ even under extreme environmental conditions, like humidity (refer to **Figure 1.2.E**).

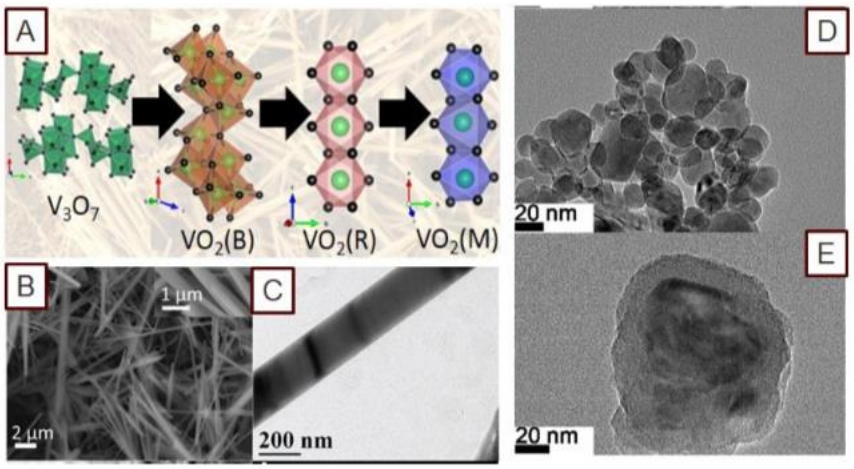


***Figure 1.2**: (A) Development of hydrothermal processing route for preparing a scalable high-quality pure phase $VO_2$ nanocrystals to be incorporated within nanocomposite thin films. (B) Scanning electron micrograph. (C) $VO_2$ nanocrystals' transmission electron micrograph through hydrothermal route. (D) Solution phase prepared $VO_2$ nanocrystals' transmission electron micrograph. (E) Deposition of $SiO_2$ shell around the $VO_2$ nanocrystals using refractive index matching.*[9,10]

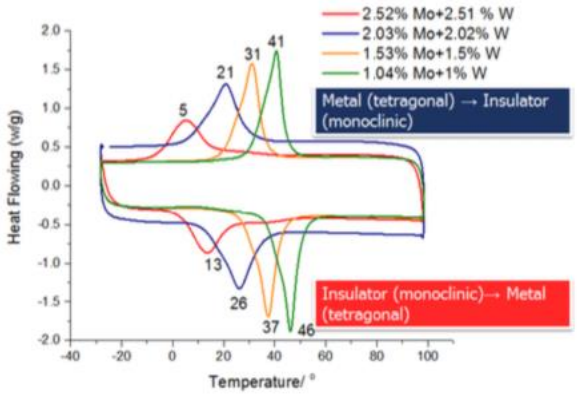


***Figure 1.3**: Modulation of transition temperature of $VO_2$ nanocrystals using differential scanning calorimetry, which is essential in measuring the ability to tune the transition temperature to room temperature for switchable fenestration.*[9,10]

The thin films portray an optical transmittance and thermally induced modulation of conductance as illustrated in **Figure 1.4.A-B**. The increase in the $VO_2$ thin films' reflectance causes the near infrared transmittance to be suppressed at high temperatures as shown on **Figure 1.4.B** whereas the visible light transmittance and the appearance of the film remains the same. In **Figure 1.4.A-B**, different loadings of $VO_2$ nanocrystals in an acrylic matrix using aqueous dispersion[8] are used to express their varying values of near infrared transmittance and visible light transmittance.

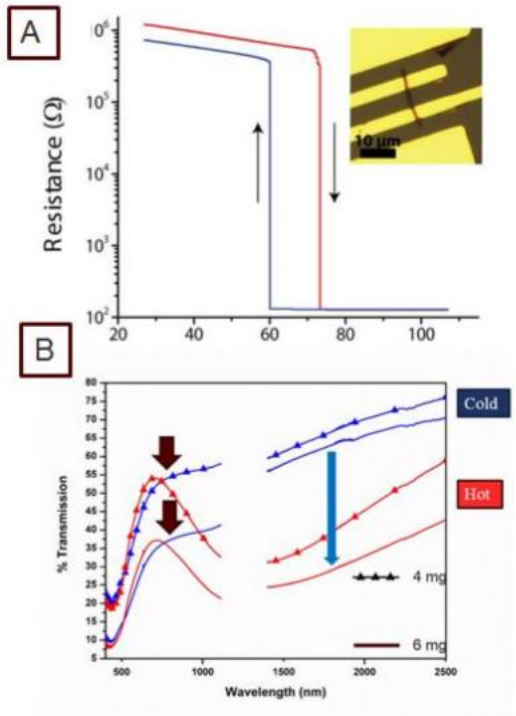


***Figure 1.4**: (A) Induced resistance modulation of $VO_2$ nanowires upon heating. (B) $VO_2$ nanocomposite thin film thermochromic performance.*[9,10]

## 1.3 Charge Transfer (CT) Based on Thermochromic Material

The thermochromic material possess tunable bands in the visible region. The visible region accounts for 50% of the solar spectrum.[12] This organic material is composed of three components: a negative-charged counter-ion, an amphiphilic π- electron-deficient *bis*-bipyridinium acceptor, and a π-electron-rich donor. The material portrays fully reversible thermochromic properties in the visible region with the range of tunable transition temperatures between 45ºC and 105ºC as shown in **Figure 1.5**.

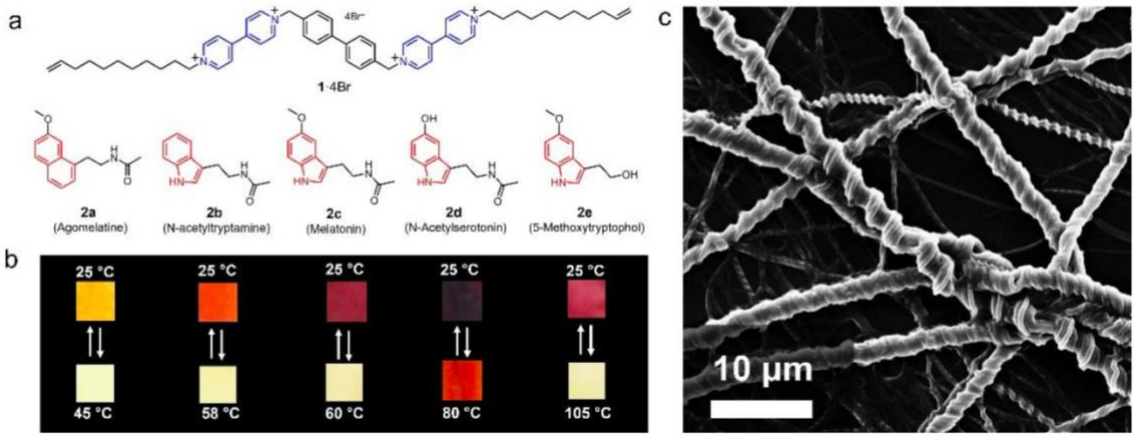


***Figure 1.5**: (A) Acceptor's 1.4Br and donors' 2a-2e structural performance. (B) Donors' 2a-2e prepared thermochromic films' photographs at room temperature and above transition temperature. (C) Images of fibrous donor-acceptor self-assembly using scanning electron microscopy.*[9,10]

The π → π* CT interactions between the donor and acceptor highly affects the materials' visible band at lower temperatures. In contrast, the n → π CT interactions between the counterion and acceptor affect the visible band at higher temperatures. The counterion-acceptor and donor-acceptor CT interactions' strength determines the thermochromic transition temperature. Therefore, the thermochromic transition temperature and colors of these materials are both easily

tailored through altering the donors and counterions. These materials have a feasible aqueous solution processability, which drastically lowers the costs, improves the manufacturing of product, and improves the fabrication compatibility.

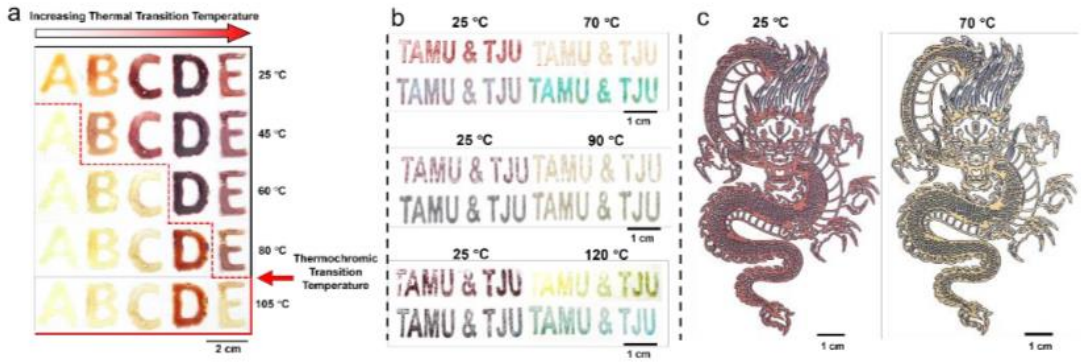


***Figure 1.6**: Different solution processing methods used to prepare thermochromic patterns at room and above transition temperatures. (A) Image of drop-casted pattern on glass substrate. (B) Image of stamped pattern on paper. (C) Image of inkjet-printing pattern on paper.*[9,10]

In **Figure 1.6**, thermochromic materials were deposited using inkjet-printing with high resolution and their ability to be tuned and processed allows them to be an optimal component in smart windows.

# 2. METHODS

A distinctive property of the developed material is the independent spectrally selective control of transmittance across the near infrared and visible regions of the solar spectrum. This thermochromic material also utilizes the nanoparticles' phase transformation and the donor-acceptor CT complexes. The used thermochromic elements ($VO_2$@$SiO_2$) were developed and integrated in a hybrid nanocomposite film. Then, they will be used to develop structure-processing-function correlations, validate energy savings, and develop prototypes.

For the synthesis of the thermochromic polymer, an iterative feedback loop will be used to combine it with the oxide nanoparticle elements along with the nanoparticle surface modification to achieve compatibility with the polymeric host matrix in relative to the nanoparticle dispersion and matching of the refractive index. Then, the use of reflectance spectroscopy and temperature-dependent multi-spectral optical absorption to assess the optical functionality. Structure-processing-function maps will be developed through characterizing the thin films' properties and stability to achieve suitable formulations for the building envelope, from translational materials to manufacturable formulations as illustrated in **Figure 2.1**.

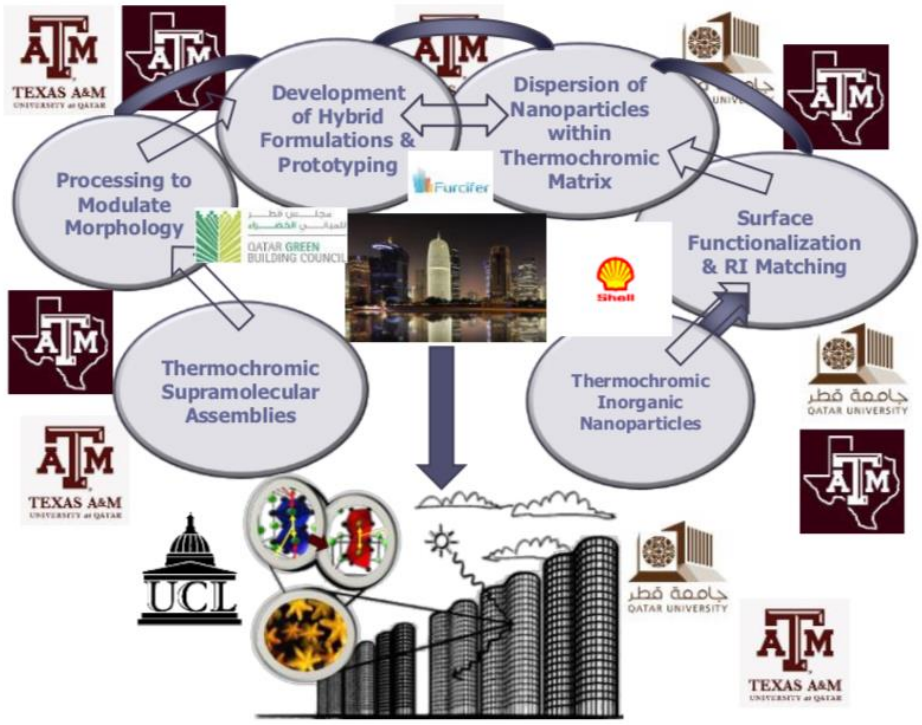


***Figure 2.1****: Methodology and connectivity of proposed tasks across the collaborative entities to develop the thermochromic material.*

## 2.1 Thermochromic Nanoparticles Synthesis Controlling the Size and Dopant Incorporation

The $VO_2$ nanoparticles are prepared through hydrothermal or aqueous dispersion methods while, simultaneously, controlling the size and dopant incorporation. The oxygen stoichiometry is controlled within a tight tolerance window to ensure a large phase transition magnitude.

## 2.2 Dispersion and Functionalization of the Surface

The implementation of the Stöber method in order to functionalize the doped $VO_2$ nanoparticles with the shells of the amorphous $SiO_2$ as shown in **Figure 1.2.E**.

## 2.3 Characterization of the Thermochromic Material

Transmission Electron Microscopy (TEM), Differential Scanning Calorimetry (DSC), and Optical Transmittance Spectra (OTS) will be used to conduct further analysis on the structure and properties of the developed thermochromic material.

# 3. RESULTS

First, the synthesis of the $VO_2$ nanocrystals are conducted via an aqueous route in which tungsten is incorporated as a dopant on the cation sublattice. This process consists of 3 steps, including the reduction of ammonium metavanadate ($NH_4VO_3$) and ammonium metatungstate hydrate($(NH_4)_6H_2W_{12}O_{40}\cdot xH_2O$) with 5 wt.% hydrazine ($N_2H_4$) in water in order to precipitate $VO(OH)_2$. The nanocrystals are annealed to increase their crystallinity to enhance their thermochromic performance. The nanocrystals are first encapsulated in $SiO_2$ shells to avoid the sintering of the nanocrystals. The $SiO_2$ shells were adjusted using the Stöber process in which the nanocrystals were dispersed in ethanol and water using ultrasonication. The $SiO_2$-encased $W_xV_{1-x}O_2$ are then removed using centrifugation and washing using acetone and ethanol is conduected, then drying under a nitrogen flow.[13]

The nanocomposite film is prepared using aqueous dispersion methods through methacrylic acid/ethyl acrylate copolymer as a continuous matrix. The characterization of the nanocrystals was conducted through D8-Focus Bragg Brentano X-ray Powder Diffractometer with a Lynxeye PSD detector and a copper Kα source $\lambda = 1.5418$ Å. The particles of the core—shell $W_xV_{1-x}O_2@SiO_2$ nanocrystals were dispersed into acetone and then drop casted on the grid. The TEM was conducted at a voltage of 200 kV and 100 mA beam current.

The nanocrystals' optical property was determined by methacrylic acid/ethyl acrylate co-polymer matrix dispersion with a loading of 0.4 – 0.9 mg/mL and then through the casting of the film on microscopic blade of thickness of 2.54 mm to dry overnight.[13]

The substitutional incorporation of W in $VO_2$ through the use of ammonium metatungstate hydrate as a dopant decreased the monoclinic insulating temperature of a value of 7ºC/at. % W incorporated in $VO_2$ as shown in **Figure 3.1A**. The temperature dependent optical transmittance is depicted in **Figure 3.2**. It shows the nanocomposite films of the W-alloyed $VO_2$ nanocrystals with varied W amount to the same film specifications through embedding ca. 0.4 mg/mL loadings of nanocrystals in methyl acrylic acid/ ethyl acrylate co-polymer cast onto a glass slide. In **Figures 3.1B-C**, the constant nanocomposite specifications and nanocrystal loadings are shown. A reduction from 28.9% for undoped $VO_2$ nanocrystal thin films to 18.9% for nanocomposite thin films containing 2.5 at. % alloyed W in $VO_2$ was observed. The NIR transmittance as a function of temperature for the films embedding the $VO_2$ nanocrystals incorporating ca. 2.5 at. % W and undoped $VO_2$ nanocrystals are shown in **Figures 3.1B-C**. It can be concluded that the NIR modulation is decreased for the alloyed sample in comparison to the unalloyed sample. The alloying amount of 2.5 at. % W has been chosen for the solid solution according to the desired temperature range for the $W_xV_{1-x}O_2$ nanocrystals.[13]

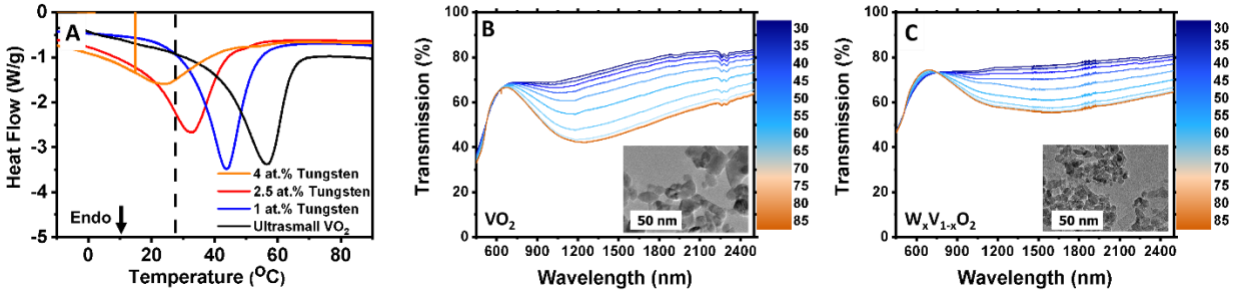


***Figure 3.1**: (A) scans of DSC for the endothermic $VO_2$ MIT doped with 0-4 at. % tungsten. (B-C) $VO_2$ IR spectra and 2.5 at. % $W_xV_{1-x}O_2$ while varying the temperature between 30ºC and 85ºC.*[13]

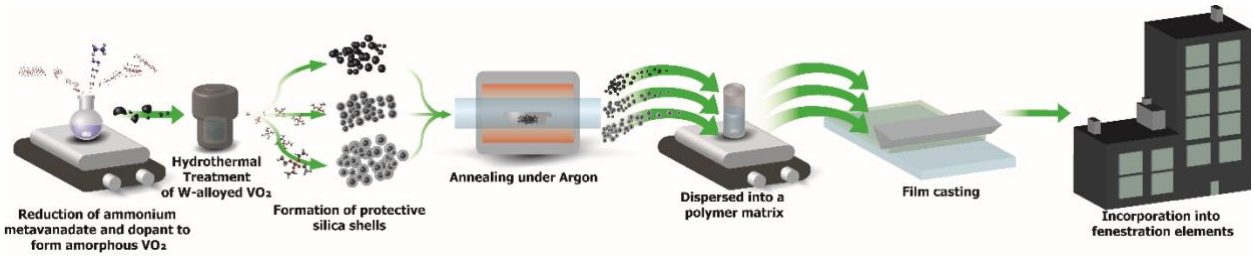


***Figure 3.2**: Synthesis of $W_xV_{1-x}O_2$ nanocrystals, followed by the encapsulation with $SiO_2$ shells, annealing under argon, dispersion in methacrylic acid/ethyl acrylate co-polymer matrix, film casting, and an evaluation of the dynamically switchable fenestration element.*[13]

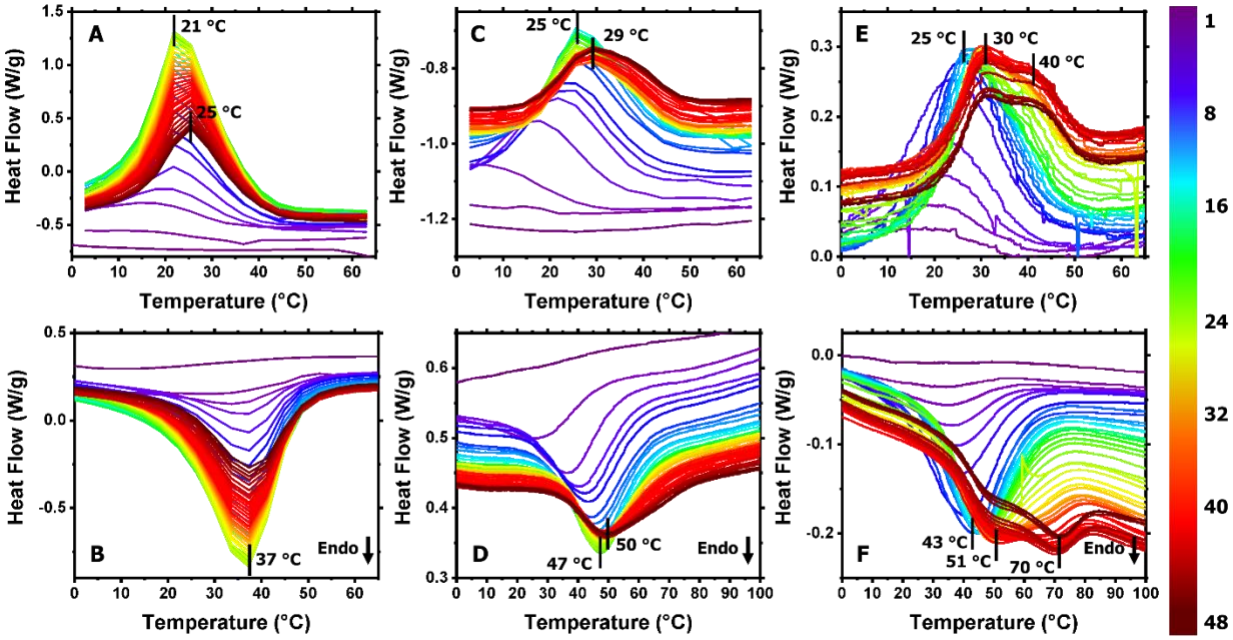


***Figure 3.3**: 2.5 at. % DSC tungsten-alloyed $VO_2$ with and without $SiO_2$ shells. (A,B) nanocrystals of $W_xV_{1-x}O_2$. (C,D) nanocrystals of $W_xV_{1-x}O_2$ with 8.1 nm $SiO_2$ shell. (E,F) $SiO_2$ of 19 nm with $W_xV_{1-x}O_2$ shell. Data of DSC has been obtained at a scan of 15ºC/min in the temperature of 20ºC-500ºC with a 30-minute isothermal*

The exothermic and endothermic features are shown in thermograms for encapsulated nanocrystals through thermal annealing in **Figure 3.3**. The maximum values are reached within 40 and 48 cycles. The transitions translate to improved crystallinity of the lattice. Atoms of tungsten distributed across the range of lattice sites in which they become trapped kinetically throughout the low-temperature condensation reactions and are able to move to more thermodynamically favored sites. A smaller dopant site distribution preference and more homogenous W alloying along the lattice yields defined transitions around the thermodynamic transition temperature of W-alloyed $VO_2$. High temperatures begin to strengthen and emerge the encapsulated crystals when increasing the annealing time. The value of transition is equivalent to ca. 70ºC and is close to the transition temperature of the bulk $VO_2$. When more annealing is performed, the dopant atoms separate to surfaces and from the W-alloyed $VO_2$ lattice. These operating conditions are deemed realistic as they allow for desired properties. The desired properties are such that the shell thickness and annealing time result in an optimal crystallinity and ultrasmall dimensions while holding a solid solution of tungsten atoms on the vanadium sublattice to allow for the near ambient temperature processing and operation.[13]

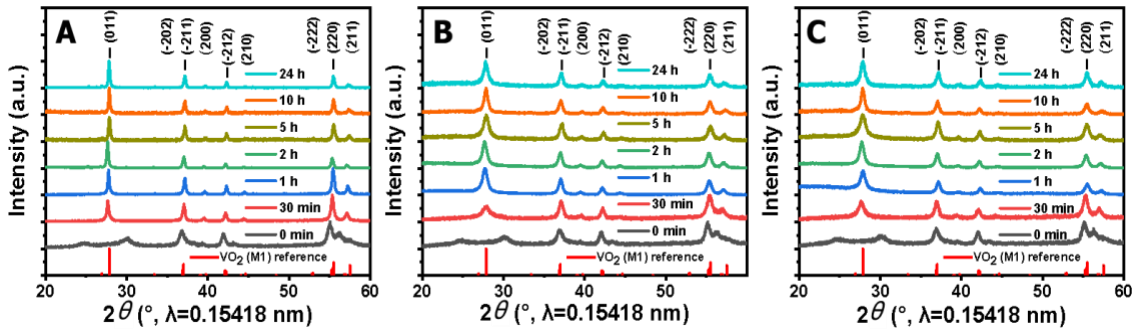


***Figure 3.4**: (A) XRD powder of $W_xV_{1-x}O_2$. (B) 8.1 nm $SiO_2$ shell with $W_xV_{1-x}O_2$. (C) 19 nm $SiO_2$ shell with $W_xV_{1-x}O_2$ under different annealing conditions in which every sample contained 2.5 at. % tungsten alloyed on the cation lattice.*[13]

The W-alloyed nanocrystals have been first encapsulated with a $SiO_2$ shell as shown in **Figure 3.2** in order to circumvent the sintering of the crystals while enhancing their crystallinity. This allows the nanocrystals to be annealed inside their individual nanoscale reactors. The deposited amorphous $SiO_2$ shells are shown in **Figure 3.4** without drastic contribution to the diffraction patterns. The $W_xV_{1-x}O_2$@$SiO_2$ nanocrystals TEM images with thickness of ca. 8.1 ± 0.9 and 19 ± 1 nm, respectively, are shown in **Figure 3.5H-N (S2 C-D) and 3.5O-U (S2 E-F).**[13]

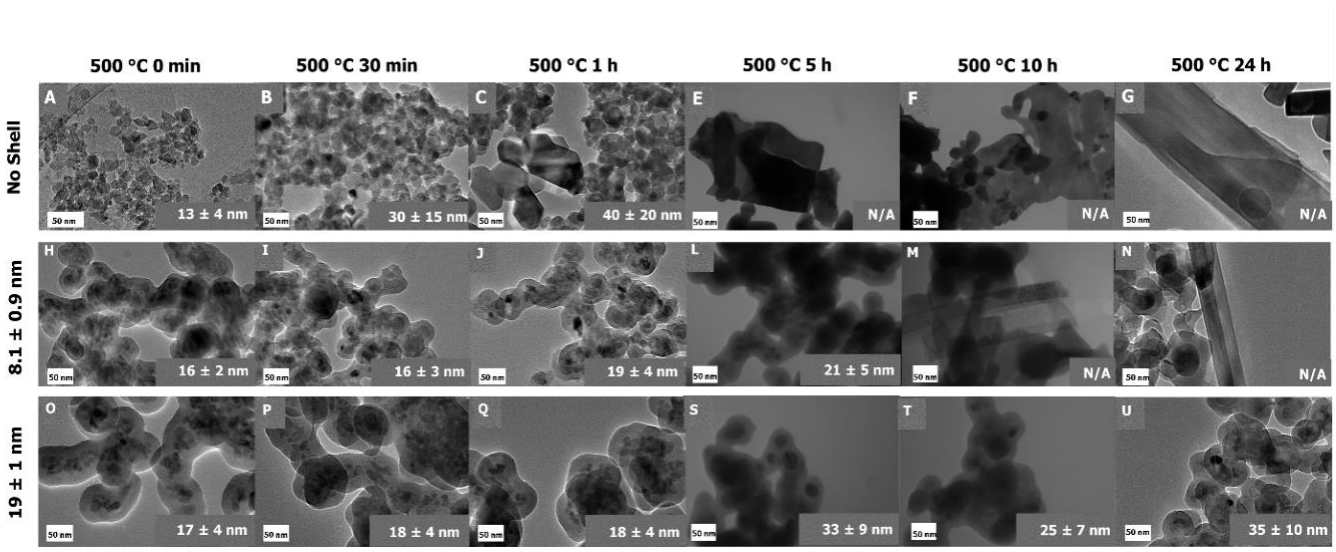


***Figure 3.5**: $W_xV_{1-x}O_2$ nanocrystals TEM images containing 2.5 at.% W : (A-G) with no shell. (H-N) 8.1 nm shell. (O-U) 19 nm shell. All under varying annealing conditions shown in the legends.*[13]

The FT-IR spectrometer and MIR and NIR radiation were used to analyze the film. The obtained spectra gave values of $\Delta T_{SOL}$, $\Delta T_{LUM}$, and $\Delta T_{NIR}$ through plotting the transmission as a function of temperature and integrating the area under the curve before and after heating. The percentage difference of the areas before and after heating was used for that purpose in the wavelength ranges of 450-2500 nm, 450-750 nm, and 750-2500 nm as shown in **Table 3.1**.[13]

***Table 3.1**: Percentage difference from optical transmittance spectra in NIR (780—2500 nm), Sol (450—2500 nm), and Lum (450—780 nm) regions of the electromagnetic spectrum.*[13]

| Sample | Annealing Time (h) | $\Delta T_{NIR}$ (%) | $\Delta T_{Sol}$(%) | $\Delta T_{Lum}$(%) | $\%T_{555\ nm}$ |
|---|---|---|---|---|---|
| No Shell | 0.5 | 1.0 | -0.5 | -8.4 | 45.8 |
| No Shell | 1 | 3.5 | 3.8 | 5.2 | 58.9 |
| No Shell | 2 | 16.0 | 12.5 | -9.3 | 42.9 |
| No Shell | 5 | 27.2 | 22.8 | -14.0 | 35.6 |
| No Shell | 10 | 14.7 | 12.0 | -4.6 | 52.5 |
| No Shell | 24 | 9.6 | 8.2 | 0.2 | 50.8 |
| 8.1 ± 0.9 nm | 0.5 | -0.2 | 0.3 | 2.9 | 49.5 |
| 8.1 ± 0.9 nm | 1 | 0.6 | 1.0 | 3.1 | 47.6 |
| 8.1 ± 0.9 nm | 2 | 2.9 | 2.6 | 1.0 | 53.6 |
| 8.1 ± 0.9 nm | 5 | 21.9 | 20.0 | 8.2 | 61.2 |
| 8.1 ± 0.9 nm | 10 | 15.0 | 14.5 | 12.0 | 76.9 |
| 8.1 ± 0.9 nm | 24 | 27.3 | 23.9 | 0.6 | 58.7 |
| 19 ± 1 nm | 0.5 | -0.2 | 0.02 | 1.2 | 45.1 |
| 19 ± 1 nm | 1 | 2.0 | 2.0 | 2.2 | 48.8 |
| 19 ± 1 nm | 2 | 0.9 | 0.9 | 0.6 | 54.3 |
| 19 ± 1 nm | 5 | 12.0 | 11.0 | -5.1 | 61.2 |
| 19 ± 1 nm | 10 | 14.8 | 12.3 | -2.6 | 70.0 |
| 19 ± 1 nm | 24 | 35.6 | 32.0 | 8.1 | 64.2 |

To find the optimal conditions in the three dimensions of the highest visible light transmittance, in which the reflectance of the ultrasmall nanocrystals is preserved. It occurs at the desired neat-ambient transition temperature, where the effective reflectance of alloying of tungsten on vanadium sites at the concentrations of 2.5 – 4 at. % is. In addition to the NIR modulation by the reflection of a crystalline alloyed lattice. In **Figure 3.6**, the data was collected for the range of 450 – 2500 nm for the temperature variant optical transmittance.[13]

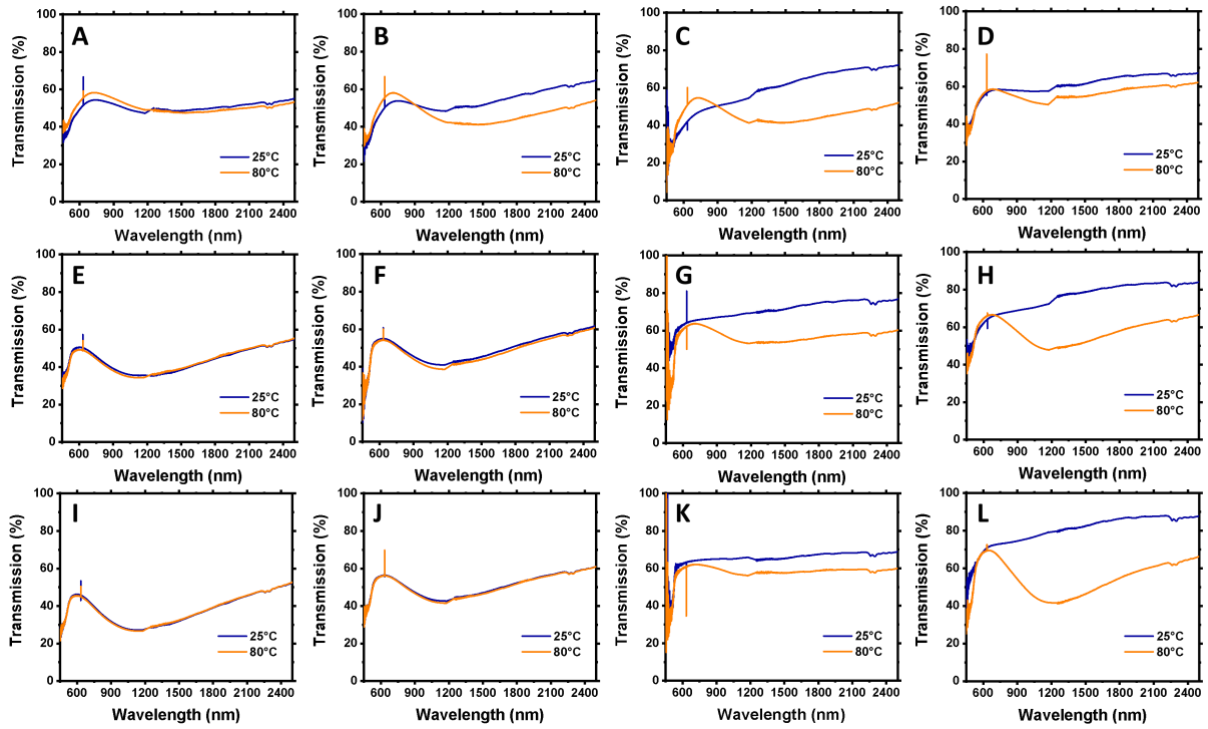


***Figure 3.6**: (A-D) Spectra for $W_xV_{1-x}O_2$ with no shell, (E-H) 8 nm shell, and 19 nm shell (I-L) at 500°C after annealing using around for (A, E, I) 30 minutes. (B, F, J) for 2 hours. (C, G, K) for 5 hours. (D, H, L) for 24 hours. Blue lines represent IR transmittance at room temperature while orange lines represent IR transmittance at high temperatures. [13]*

A high NIR modulation of $\Delta T_{NIR}$ of ca. 27.2% for the unencapsulated nanocrystals can be reached after 5 hours of annealing in addition to the visible light transmittance of 35.6% at 555 nm.[13] In **Figure 3.3 (A-B)** and **Table 3.1**, it is shown that the transition of heating is centered at 29.6ºC. Contrary to the behavior of the encapsulated nanocrystals, the extra protection from the silica shell allows for a maximum NIR modulation (ca. 27.3%) to be reached for 8.1 nm (ca. 27.3%) and 19 nm (ca. 35.6%) of $SiO_2$ shell thickness after 24 hours of annealing. The NIR modulation was improved and increased from 58.7% to 64.2% at 555 nm.[13] The unencapsulated nanocrystals' NIR modulation tapers off quickly while the nanocrystals grow causing scattering mechanism to occur. This results in the decrease in the ability to modulate the NIR transmittance as the LSPR features starts to disappear.[13] When the annealing time of 24 hours is reached in **Figure 3.6D**, the large agglomerates' scattering mechanisms are enough to prevent the nanocrystals from significantly modulating the NIR transmittance.[13]

# 4. CONCLUSION

The thermochromic fenestration elements were made from $VO_2$ nanoparticles and they require control over the crystal's alloying, dimensions, and crystallinity to attain the desired combination of high visible light transmittance, high NIR modulation, and near-ambient temperature operational range. [13] An analysis and study of the synthesis and annealing of the $W_xV_{1-x}O_2$ nanocrystals was conducted in this paper. The utilization of the XRD, TEM, DSC, and optical transmittance data was to study the use of two different silica shell thickness and different annealing points and their effect on the nanocrystal crystallinity, size, and dopant solvation. It was concluded that a higher annealing time, while keeping the particles ultrasmall through $SiO_2$ shell, encapsulation is needed to obtain high crystallinity of $W_xV_{1-x}O_2$.[13] Over extended annealing of the nanocrystals is unfavored as it forces a practical limit to the processing conditions. The optimal processing conditions were found to be at 15 hours of annealing time at the temperature of 500ºC under an argon constant flow with an 8.1 nm $SiO_2$ shell. The obtained results were $\%T_{555}$ nm of 78% with a $\Delta T_{NIR}$ of 26% [13] with a particle loading of 0.8 mg/mL in the nanocomposite films (W-alloyed nanocrystals) embedded in the methacrylic acid/ethyl acrylate co-polymer matrix.[13] This work is important in overcoming the challenges associated with the design of the fenestration elements in terms of the alloy design, encapsulation, and processing conditions. Furthermore, the onset temperature can be altered (depressed) in order to allow for the use in different climates and other desired temperatures through the increase in the dopant concentration.[13]

# REFERENCES


[1] U.S. Department of Energy, Energy Efficiency Trends in Residential and Commercial Buildings, **2008**.

[2] American Council for an Energy Efficient Economy, Cooling Systems, **2015**. http://www.aceee.org/consumer/cooling.

[3] Kanu, S. S.; Binions, R., Thin films for solar control applications. *Proceedings of the Royal Society A: Mathematical, Physical and Engineering Science* **2010**, 466, 19-44.

[4] Smart glass and Windows 2018-2028: Electronic shading and semi-transparent PV, **2003**. https://www.idtechex.com/en/research-report/smart-glass-and-windows-2018-2028-electronic-shading-and-semi-transparent-pv/601.

[5] World's most adopted Dynamic Glass: Suntuitive dynamic glass. **2018**. https://suntuitiveglass.com/.

[6] Smart Window Technology. **2010**. https://www.ravenwindow.com/.

[7] Chang, T.-C. *Review on Thermochromic Vanadium Dioxide Based Smart Coatings: from Lab to Commercial Application*. **2018**.

[8] Fleer, N. A.; Pelcher, K. E.; Zou, J.; Nieto, K.; Douglas, L. D.; Sellers, D. G.; Banerjee, S., Hybrid Nanocomposite Films Comprising Dispersed VO2 Nanocrystals: A Scalable Aqueous-Phase Route to Thermochromic Fenestration. *ACS Appl. Mater. Interfaces* **2017**, 9, 38887-38900.

[9] Whittaker, L.; Patridge, C. J.; Banerjee, S., Microscopic and Nanoscale Perspective of the Metal−Insulator Phase Transitions of VO2: Some New Twists to an Old Tale. *The Journal of Physical Chemistry Letters* **2011**, 2, 745-758.

[10] Whittaker, L.; Jaye, C.; Fu, Z.; Fischer, D. A.; Banerjee, S., Depressed Phase Transition in Solution- Grown VO2 Nanostructures. *Journal of the American Chemical Society* **2009**, 131, 8884-8894.

[11] Alivio, T. E. G.; Sellers, D. G.; Asayesh-Ardakani, H.; Braham, E. J.; Horrocks, G. A.; Pelcher, K. E.; Villareal, R.; Zuin, L.; Shamberger, P. J.; Arróyave, R.; Shahbazian-

Yassar, R.; Banerjee, S., Postsynthetic Route for Modifying the Metal—Insulator Transition of VO2 by Interstitial Dopant Incorporation. *Chemistry of Materials* **2017**, 29, 5401-5412.

[12] Gorgolis, G.; Karamanis, D., Solar energy materials for glazing technologies. *Solar Energy Materials and Solar Cells* **2016**, 144, 559-578.

[13] Al-Hashimi, M. Near-Ambient Nanocomposite Thermochromic Fenestration Elements from Post-Encapsulation-Annealed Tungsten-Alloyed Vanadium(IV) Oxide Nanocrystals. *ACS Publications **2022***.